Brilliance
Research of Artificial Intelligence

E-ISSN : 2807-9035
Volume 6, **Number** 4, November 2026
https://doi.org/10.47709/brilliance.v6i4.9749

AI-Based Prediction of Water Vapor Changes from Kalimantan Forest Fires Using Terra MODIS Imagery

Oktalia Trianandа Lovita[1*], Zharifah Muthi'ah[2], Mohd. Iqbal Muttaqin[3], Mulyati[4], Khairunnisa[5]
[1,2,3,4,5]Universitas Bina Bangsa Getsempena, Indonesia,
[1]oktalia@bbg.ac.id, [2]zharifah@bbg.ac.id, [3]iqbalmuttaqin@bbg.ac.id, [4]mulyati@bbg.ac.id, [5]khairunnisastr@bbg.ac.id

open access

***Corresponding Author**

Article History:
Submitted: 06-10-2026
Accepted: 13-10-2026
Published: 01-11-2026

Keywords:
Water Vapor; GPS CORS; weather; TERRA MODIS.

Brilliance: Research of Artificial Intelligence is licensed under a Creative Commons Attribution-NonCommercial 4.0 International (CC BY-NC 4.0).

ABSTRACT

The weather changes from forest fires in Kalimantan resulted in the earth's changing very ekstrim. Water Vapor or Vapor is a manifestation of water in the form of gas. It is still a job has been difficult for researchers atmosphere. Global Positioning System (GPS) in the troposphere and are equipped with surface data, this study used 8 (eight) GPS stations Kalhutra GPS Array (SuGAR) and 2 (two) points which is the world IGS CORS station. This method is called inversion GPS, while the TERRA MODIS satellite imagery used methods transmittance. From the experiments conducted in this research process, obtained. From the results of plotting graphs of temporal variations, it is known that the average moisture content in the dry months ranged from 56.59 mm to 38.95 mm, while the wettest months in this case because the graph ranges from 58.71 mm to 47.72 mm. The obtained results from average Water Vapor during the fire that was in 2010 ranged from 70.26% in 2011 ranged between 84.49% and in 2026 ranged from 90.15%, but the correlation (r) between the Water Vapor from TERRA MODIS satellite imagery and GPS is quite high. Based on forest fires, MODIS estimate the humidity around 54-77%. But Water Vapor obtained TERRA MODIS satellite imagery ranges between ± 3-8 cm / day is ± 89.49%. Then it will affect human health, because it influences the weather cycle in Indonesia.

INTRODUCTION

Climate change is a global phenomenon characterized by shifts in temperature and precipitation patterns. Human activities, principally through greenhouse gas (GHG) emissions, have unequivocally caused global warming, with global surface temperature reaching 1.1°C above the 1850–1900 level in 2011–2020 (IPCC, 2023). Global surface temperature has also risen faster since 1970 than in any other 50-year period over at least the last 2,000 years (IPCC, 2023). The main driver is the continued accumulation of GHGs in the atmosphere.

In 2024, the globally averaged surface concentrations of carbon dioxide (CO_2), methane (CH_4), and nitrous oxide (N_2O) reached unprecedented highs of 423.9 ppm, 1942 ppb, and 338.0 ppb, respectively (WMO, 2025). These gases absorb long-wave radiation, so higher concentrations raise the Earth's surface temperature (Vaquero-Martínez & Antón, 2021).

Water vapor (H_2O) is dynamic in both space and time, so measuring its content is an important but challenging task. Satellite sensors such as Terra MODIS provide spatially continuous PWV (Zhu et al., 2021). Their accuracy varies by region and product. Over mainland China, MODIS PWV accuracy was reported as better than 4.3 mm, with the near-infrared product generally outperforming the infrared one (Zhao et al., 2022).

GPS technology can be used to estimate atmospheric water vapor, an approach known as GPS (or GNSS) meteorology, which was first proposed by Bevis et al. (1992, as cited in Vaquero-Martínez & Antón, 2021). For example, Zhu et al. (2021) used GNSS-PWV from 246 stations, together with ERA5 reanalysis, to evaluate MODIS near-infrared PWV over China, and their calibration model improved its precision by 94% and accuracy by 53%.

This finding is further supported by more recent studies. GNSS-derived PWV is commonly used as the reference for evaluating other PWV products (Su et al., 2021). Vaquero-Martínez and Antón (2021) describe GNSS meteorology as a reliable, low-cost, weather-independent method with high temporal resolution and high accuracy. Zhu et al. (2021) used GNSS-PWV together with ERA5 reanalysis to evaluate MODIS near-infrared PWV over China, and their calibration model improved its precision by 94% and its accuracy by 53%. In Sumatra, Feng et al. (2021) showed that a regional continuous GPS network can be used to study intra-seasonal variability in water vapor, using zenith wet delay (ZWD) time series from geodetic-quality processing as a proxy for PWV, without auxiliary meteorological data. Consequently, GPS-based observation holds promise for providing accurate, continuous, local-scale water vapor data.

Zenith Tropospheric Delay (ZTD) is the total delay that the troposphere imposes on a GPS signal in the zenith direction, and it consists of the zenith hydrostatic delay (ZHD) and the ZWD (Vaquero-Martínez & Antón, 2021). GPS positioning must account for this delay, so ZTD is essential for correcting tropospheric effects when determining the precise position of a point. For meteorological purposes, ZHD is computed from meteorological data, typically surface

This is an Creative Commons License This work is licensed under a Creative Commons Attribution-NonCommercial 4.0 International License.

Brilliance
Research of Artificial Intelligence

E-ISSN : 2807-9035
Volume 6, **Number** 4, November 2026
https://doi.org/10.47709/brilliance.v6i4.9749

pressure, and subtracted from ZTD. The remaining ZWD is caused only by water vapor and is converted into PWV (Vaquero-Martínez & Antón, 2021). In this research, ZTD is therefore used to determine PWV within the troposphere.

This study uses the Sumatran GPS Array (SuGAr), a continuous GPS network maintained by the Earth Observatory of Singapore to monitor tectonic deformation and earthquakes along the Sumatra subduction zone (Earth Observatory of Singapore, n.d.). Although it was built for tectonic studies, the network has also proven useful for atmospheric water vapor research (Feng et al., 2021). The GPS observation data are processed with GAMIT/GLOBK, the scientific software developed by the Massachusetts Institute of Technology, to determine ZTD and PWV at the study site. GAMIT/GLOBK has been used to estimate ZWD from permanent GNSS stations and to validate it against radiosonde-derived data (Zhai et al., 2022). MODIS imagery, with its extensive spectral capabilities, is a compelling subject for research. Terra MODIS acquires data in 36 spectral bands from 0.4 to 14.4 µm at spatial resolutions of 250 m, 500 m, and 1 km (NASA, n.d.). PWV derived from its near-infrared water vapor channels has a higher spatial resolution than point-based GNSS and radiosonde measurements, but it suffers from missing data and poor accuracy under cloudy conditions (Wang et al., 2024).

LITERATURE REVIEW

The Concept of Weather Change

Weather refers to the state of the atmosphere at a specific time and within a relatively small area over a short duration. It is formed by a combination of weather elements, and weather conditions can persist for only a few hours such as morning, midday, or afternoon varying by location and time. In Indonesia, weather conditions are typically announced for a 24-hour period through forecasts developed by the Meteorology, Climatology, and Geophysics Agency (BMKG) and the Ministry of Transportation. In developed nations, weather updates are issued hourly with a high degree of accuracy. The scientific study of weather is known as meteorology. It is defined as the state of the atmosphere expressed through values of various parameters such as temperature, pressure, wind, humidity, and precipitation phenomena at a specific location or region over a short timeframe (ranging from minutes, hours, days, and months to seasons or years).

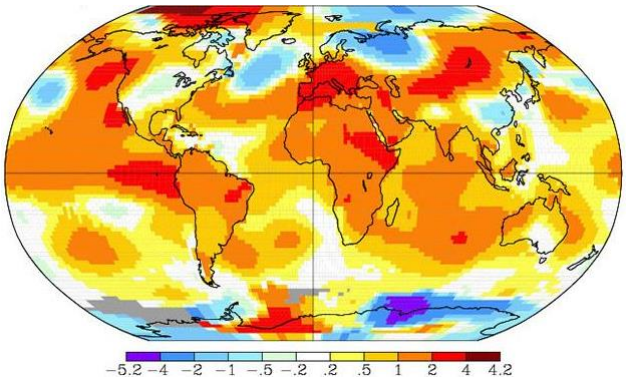


Figure 1. Weather formation occurring in Indonesia (NASA, 2025)

Figure. 1 Forest fires can cause massive losses in a short period, far exceeding the damage caused by other factors affecting forests. The causes of forest fires vary, stemming from both natural sources and human activities; indeed, human-induced fires are the primary cause of forest fires in Indonesia.

Global warming additionally increases the atmosphere's water-holding capacity and further intensifies wet extremes (Hsu et al., 2025). Rainfall therefore serves as an indicator of changing weather conditions: its fluctuations relative to monthly or annual averages, together with its intensity, reflect these changes. Atmospheric water vapor is closely tied to this process. In tropical Thailand, GNSS-derived precipitable water vapor (PWV) increased significantly during flood events, indicating its potential as an anticipatory indicator of impending rainfall (Trakolkul et al., 2024).

Global Positioning System (GPS)

(Navigation Satellite Timing and Ranging Global Positioning System) NAVSTAR GPS is a satellite-based radio navigation system that provides precise positioning, navigation, and timing information to users. The system is continuously available worldwide and operates independently of weather conditions. Definition. GPS is a U.S.-owned utility that provides positioning, navigation, and timing (PNT) services through three segments: space, control, and user (GPS.gov, n.d.-a). GPS is the oldest of the global GNSS constellations and is the system the right panel of your previous figure is modeled on.

1. Space Segment. The nominal constellation has 24 operating satellites. They transmit one-way signals carrying the satellite's position and time (GPS.gov, n.d.-a). In practice the constellation is larger than the baseline. In late 2022 it had 37 satellites, 31 of them set healthy, with five GPS III satellites declared operational (Baker, 2022).

This is an Creative Commons License This work is licensed under a Creative Commons Attribution-NonCommercial 4.0 International License.

Brilliance
Research of Artificial Intelligence

E-ISSN : 2807-9035
Volume 6, **Number** 4, November 2026
https://doi.org/10.47709/brilliance.v6i4.9749

2. Control Segment. A worldwide network of monitor and control stations keeps the satellites in their proper orbits and adjusts their clocks. It also uploads updated navigation data and tracks the health of the constellation (GPS.gov, n.d.-a).
3. User Segment. This is the receiver equipment. It uses the transmitted signals to calculate the user's three-dimensional position and time (GPS.gov, n.d.-a). GPS served more than 6 billion users in 2022, with an estimated economic benefit of about $1.4 trillion (Anderson, 2022).

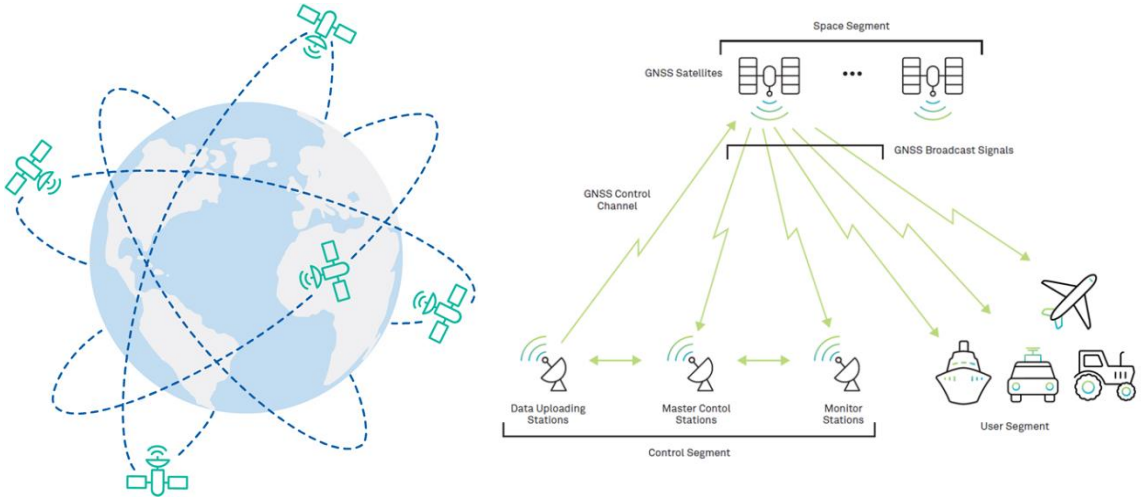


Figure 2. (a) GPS satellite constellation. (b) Basic principle of using GPS (NASA, 2021)

Figure 2(a)(b). Multi-constellation use. The four global systems are GPS (USA), GLONASS (Russia), Galileo (EU), and BeiDou (China). Using signals from all four together reduces the risk of losing service from any single system and improves reliability (NewSpace Economy, 2024). Hybrid multi-GNSS receivers can also improve accuracy, resilience, and redundancy (Mustafovski & Petrovski, 2025).

Determination of ZTD and PWV using GAMIT 10.4

GAMIT (GNSS at MIT) is a collection of programs for processing GNSS phase data. It was developed by the Massachusetts Institute of Technology, the Scripps Institution of Oceanography, and Harvard University with support from the U.S. National Science Foundation. GAMIT estimates three-dimensional relative positions of ground stations, satellite orbits, atmospheric zenith delays, and Earth orientation parameters, and it is designed to run under any UNIX operating system (MIT Technology Licensing Office. Its estimation program applies a weighted least-squares algorithm to doubly differenced phase observations, solving for relative station positions, orbital and Earth-rotation parameters, zenith delays, and phase ambiguities. The resulting estimates and their covariance matrices, called "quasi-observations," are then combined with other solutions by GLOBK, a Kalman filter, to estimate positions and velocities. GAMIT/GLOBK is widely used as high-precision GNSS data-processing software, for example in monitoring crustal deformation, tsunamis, and icebergs (Li, 2021). It has also been used to estimate zenith wet delay from permanent GNSS stations and to validate the results against radiosonde-derived data (Zhai et al., 2022).

Determination of ZTD

Zenith Tropospheric Delay (ZTD), also referred to as the atmospheric zenith delay in GAMIT, is the total delay that the neutral atmosphere imposes on a GNSS signal in the vertical direction. Because signals arrive at different elevation angles, the slant delay is expressed through zenith delays and mapping functions (Vaquero-Martínez & Antón, 2021). GAMIT, which estimates atmospheric zenith delays together with station positions, satellite orbits, and Earth orientation parameters, models the atmospheric delay at elevation angle EL as:

$$ATDEL(EL) = DRYZEN * DRYMAP(EL) + WETZEN * WETMAP(EL)\ldots\ldots(1)$$

Description:
ATDEL = Atmospheric delay (ZTD)
DRYZEN = hydrostatic component delay
DRYMAP = hydrostatic component mapping function
WETZEN = non-hydrostatic component delay
WETMAP EL = satellite elevation
EL = non-hydrostatic component mapping function

This is an Creative Commons License This work is licensed under a Creative Commons Attribution-NonCommercial 4.0 International License.

Brilliance
Research of Artificial Intelligence

E-ISSN : 2807-9035
Volume 6, **Number** 4, November 2026
https://doi.org/10.47709/brilliance.v6i4.9749

Precipitable Water Vapor

The Role of Water Vapor in Weather Systems Water vapor acts as the link between the surface and the atmosphere within the water or hydrological cycle. As shown in Figure 3, nearly all atmospheric water vapor originates at the Earth's surface, where water evaporates from oceans and continents due to solar radiation, and is released into the atmosphere by plants and animal respiration.

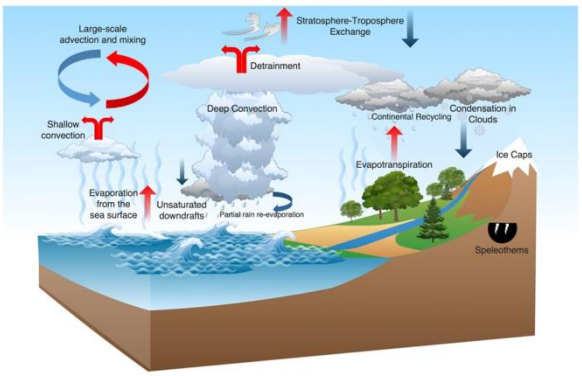


Figure 3. The Role of Water Vapor in Daily Life (NASA, 2021)

Figure. 3 Water vapor is the gaseous form of water and a trace gas of the Earth’s atmosphere (Vaquero-Martínez & Antón, 2021). The amount of water vapor in the air, referred to as humidity, can be expressed in several ways. These include the mixing ratio (grams of water per gram of dry air, commonly written in g/kg), relative humidity (the ratio of the actual amount of water vapor to the amount required to saturate the air), and other measures of concentration (Vaquero-Martínez & Antón, 2021). Water vapor plays an important role in the global water and energy cycle (Wang et al., 2024) and a key role in the Earth’s radiative balance and hydrological cycle (Zhu et al., 2021).

The TERRA MODIS Satellite

The Earth Observing System (EOS) is a NASA Earth science mission. The EOS AM satellite recently named TERRA was launched in December 1999. TERRA carries five remote sensing instruments, including MODIS and ASTER. Bands The VNIR and SWIR sensors have spectral bandwidths in the order of 10. By pointing at the same target twice, ASTER can acquire high-resolution stereo imagery. The Earth Observing System (EOS) is a flagship NASA Earth science initiative designed for long-term global observations of the land surface, biosphere, atmosphere, and oceans. The EOS AM-1 satellite, officially named Terra, Terra acts as a primary multi-sensor platform carrying five state-of-the-art remote sensing payloads MODIS (Moderate Resolution Imaging Spectroradiometer) Sensor Architecture: ASTER and MODISASTER, a collaborative payload developed by Japan's Ministry of Economy, Trade, and Industry (METI) and NASA, captures high-spatial-resolution data across 14 spectral bands spanning three sub-systems: Visible and Near-Infrared (VNIR): 3 spectral bands (0.52–0.86 µm) operating at a 15 m spatial resolution. Shortwave Infrared (SWIR): 6 spectral bands (1.60–2.43 µm) operating at a 30 m spatial resolution, optimal for lithological discrimination and alteration mineral mapping. Thermal Infrared (TIR): 5 spectral bands (8.125–11.65 µm) operating at a 90 m spatial resolution for surface temperature and emissivity retrieval.MODIS complements ASTER by collecting broader, daily-to-biennial global observations across 36 spectral bands (0.4–14.4 µm) at spatial resolutions of 250 m, 500 m, and 1,000 m.3. Stereoscopic Imagery and DEM GenerationUnlike across-track multi-pass systems, ASTER achieves high-resolution Digital Elevation Model (DEM) generation through along-track optical stereoscopy: Dual-Telescope Design: The VNIR system includes two independent telescopes in Band 3 (0.76–0.86 µm)—a nadir-looking sensor (Band 3N) pointing straight down and a backward-looking sensor (Band 3B) tilted at a 27.6° off-nadir angle. Near-Simultaneous Stereo Pair Acquisition: As the satellite moves along its orbital path, Band 3B captures the exact same ground target approximately 60 seconds after Band 3N. Topographic Extraction: Acquiring both stereoscopic views within a one-minute window minimizes atmospheric variations and temporal decorrelation, enabling precise extraction of parallax and terrain elevation (e.g., ASTER GDEM and AST14DEM products).

This is an Creative Commons License This work is licensed under a Creative Commons Attribution-NonCommercial 4.0 International License.

Brilliance
Research of Artificial Intelligence

E-ISSN : 2807-9035
Volume 6, **Number** 4, November 2026
https://doi.org/10.47709/brilliance.v6i4.9749

Table 1. Characteristics of the MODIS Satellite

Criteria	Characteristics
Type Orbit	Sun – Sychrounus, Near, Polar, Culcular
Field Of View	2.330 Km
Height	705 Km
Quantitie	12 Bit
Spacial	250 M
Resolutions	500 M
	1000 M
Resolusi	36 Kanal

Source: (http://modis.gsfc.nasa.gov)

The MODIS sensor aboard the Terra satellite captures electromagnetic radiation in 36 spectral bands (36 wavelength intervals), ranging from 0.405 µm to 14.385 µm (1 µm = 1/1,000,000 m). The number and width of these wavelength intervals define the sensor's spectral resolution, whereas pixel size defines its spatial resolution. Bands 1–2 have a spatial resolution of 250 m, bands 3–7 have 500 m, and bands 8–36 have 1,000 m. Terra crosses the equator at about 10:30 a.m. local time on its descending node, and MODIS views the entire Earth's surface every 1 to 2 days. These resolutions are suitable for regional studies. However, MODIS near-infrared PWV suffers from missing data and poorer accuracy under cloudy conditions (Wang et al., 2024), so it is commonly evaluated against GNSS-derived PWV (Zhu et al., 2021). The following table lists the Terra MODIS spectral bands (NASA, n.d.).

Table 2. MODIS Bands and Their Uses

Primary Use	Band	Bandwidth[1]	Spectral Radiance[2]	Required SNR[3]
Land/Cloud/Aerosols Boundaries	1	620 - 670	21.8	128
	2	841 - 876	24.7	201
Land/Cloud/Aerosols Properties	3	459 - 479	35.3	243
	4	545 - 565	29.0	228
	5	1230 - 1250	5.4	74
	6	1628 - 1652	7.3	275
	7	2105 - 2155	1.0	110
Ocean Color/ Phytoplankton/ Biogeochemistry	8	405 - 420	44.9	880
	9	438 - 448	41.9	838
	10	483 - 493	32.1	802
	11	526 - 536	27.9	754
	12	546 - 556	21.0	750
	13	662 - 672	9.5	910
	14	673 - 683	8.7	1087
	15	743 - 753	10.2	586
	16	862 - 877	6.2	516
Atmospheric Water Vapor	17	890 - 920	10.0	167
	18	931 - 941	3.6	57
	19	915 - 965	15.0	250

Source: (http://MODIS.gsfc.nasa.gov)

The reflectance of each object exhibits specific characteristics across different spectral channels, allowing objects to be distinguished from one another. Vegetation characteristics can be identified by comparing the red band spectrum with the near-infrared spectrum.

Derivation of Water Vapor Values

Solar radiation between 0.86 and 1.24 µm along the sun–surface–sensor path is affected by atmospheric water vapor absorption, aerosol scattering, and surface reflection. Near 1 µm, Rayleigh scattering is negligible and the main contribution to path radiance is scattering by aerosols. The absorption and scattering properties of the atmosphere and the surface must therefore be taken into account when deriving column water vapor (NASA, n.d.-a). The algorithm uses ratios of absorption channels to window channels, which partially remove the effects of surface reflectance varying with wavelength and yield the atmospheric water vapor transmittance. Column water vapor is then derived from the transmittance using theoretical radiative transfer calculations and look-up tables (NASA LAADS DAAC, n.d.).

MODIS channels 2, 5, 17, 18, and 19, centered at 0.865, 1.24, 0.905, 0.936, and 0.940 µm, respectively, are used to determine total column water vapor (Table 1). The 0.865 and 1.24 µm channels are non-absorption (atmospheric window) channels. The 0.936, 0.940, and 0.905 µm channels are water vapor absorption channels with decreasing absorption coefficients, so channel 18 (0.936 µm) is the strongest and channel 17 (0.905 µm) the weakest. The strongly

This is an Creative Commons License This work is licensed under a Creative Commons Attribution-NonCommercial 4.0 International License.

Brilliance
Research of Artificial Intelligence

E-ISSN : 2807-9035
Volume 6, **Number** 4, November 2026
https://doi.org/10.47709/brilliance.v6i4.9749

absorbing 0.936 µm channel is most useful under dry conditions, whereas the weakly absorbing 0.905 µm channel is most useful under very humid conditions or at low solar elevation (NASA, n.d.-a). Over mainland China, the NIR product generally performed better than the infrared product (Zhao et al., 2022). It has been evaluated against GNSS-derived and ERA5 PWV (Zhu et al., 2021), but it suffers from missing data and poorer accuracy under cloudy conditions (Wang et al., 2024).

Table 3. Positions and bandwidths of the MODIS IR channels used to detect water vapor.

Kanal Modis	Posision (µM)	Bandwith (µM)	Characteristic
2	0,865	0,040	Non Absorbs
5	1,240	0,020	Non Absorbs
17	0,905	0,030	Absorbs
18	0,936	0,010	Absorbs
19	0,940	0,050	Absorbs

Source: (NASA MODIS Atmosphere. https://atmosphere-imager.gsfc.nasa.gov/products/water-vapor/algorithm-overview)

Atmospheric water vapor transmittance can be accurately derived by comparing surface reflectance between an absorption channel and a non-absorption channel, while neglecting the effects of surface reflectance variations. If surface reflectance remains constant across wavelengths, a two-channel ratio is sufficient to derive water vapor transmittance. For example, transmittance in channel 19 (0.94 µm) can be obtained using Equation (2) below:

$$Tabs = 0{,}94(\mu M) = \frac{0{,}946\ (\mu M)}{0{,}865\ (\mu M)} \quad \text{.....(2)}$$

Where
Tabs = Transmittance in the absorption channel;
ρ* = Reflectance measured at the sensor. Most land surfaces are covered by soil, rock, vegetation, snow, or ice.

Recent studies have further advanced satellite-derived precipitable water vapor (PWV) retrieval by refining the relationship between near-infrared (NIR) water vapor transmittance and atmospheric water vapor content. Figure 4 illustrates the conceptual relationship between PWV and water vapor transmittance derived using the two-channel ratio method, which provides a basis for estimating atmospheric water vapor content from satellite observations (Ma et al., 2022; Zhao et al., 2024; Zhou & Cheng, 2025). PWV and the water vapor transmittance obtained via the two-channel ratio method is shown in Figure. 4 below.

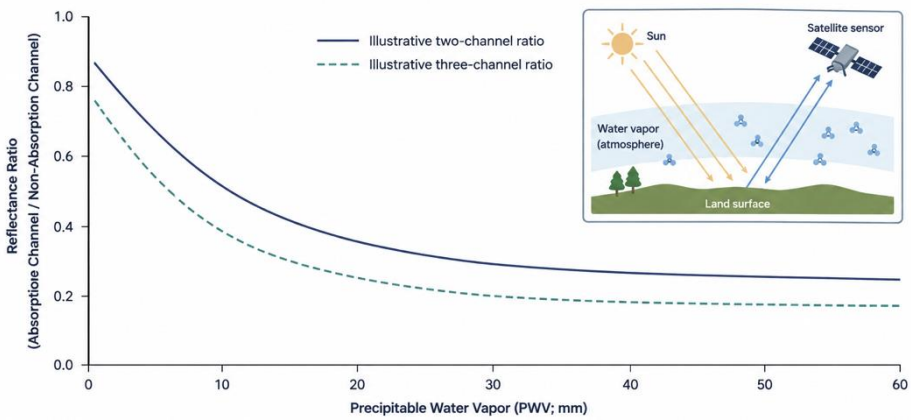


Figure 4. Simulation of the reflectance ratio of two channels (absorption channel/non-absorption channel) as a function of the amount of precipitable water along the sun-surface-sensor path (Zhao et al.(2024).

METHOD

Research Location

This study analyzes weather changes on the island of Kalimantan resulting from forest fires, utilizing GPS water vapor data and TERRA MODIS satellite imagery. Kalimantan is the sixth-largest island in the world, located in Indonesia, with an area of 114.249738km². Astronomically, Sumatra is situated between 0.874056, °E longitude.

This is an Creative Commons License This work is licensed under a Creative Commons Attribution-NonCommercial 4.0 International License.

Brilliance
Research of Artificial Intelligence

E-ISSN : 2807-9035
Volume 6, **Number** 4, November 2026
https://doi.org/10.47709/brilliance.v6i4.9749

Research Methodology

Processing Stages

The stages carried out in this research are:

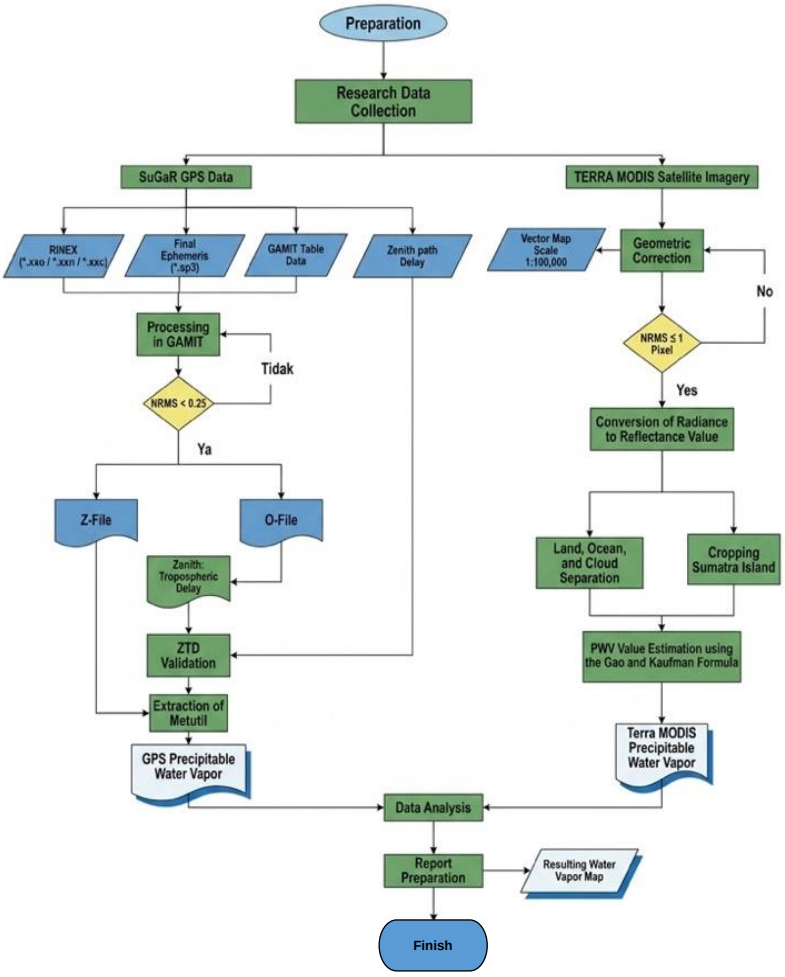


Figure 5. Flowchart of research stages.

Figure. 5 The data are obtained from two main sources: ground-based observations and Terra MODIS satellite imagery. The collected data undergo preprocessing, including data quality checking, geometric correction, and atmospheric analysis. Water vapor and other relevant satellite-derived parameters are then processed to generate thematic information. Next, the processed datasets are integrated and analyzed to identify relationships between atmospheric water vapor, land-surface conditions, and the observed environmental phenomena. The results are evaluated and validated before being presented as the final research outputs. Overall, the flowchart demonstrates a systematic workflow combining ground-based measurements, satellite remote sensing, data processing, and validation to produce reliable research results.

RESULT

Validation of ZTD Results from GPS Observation Data

This validation aims to assess the quality of the ZTD values derived from the processing of GPS observation data. The validation is conducted by comparing the ZTD values obtained from GAMIT processing at IGS stations (CBLS and CBLA) with the ZTD values provided by the IGS Troposphere Working Group. Figure 4.1 illustrates the validation of the Zenith Tropospheric Delay (ZTD) results derived from GAMIT processing against the ZTD results provided by the Troposphere Working Group.

This is an Creative Commons License This work is licensed under a Creative Commons Attribution-NonCommercial 4.0 International License.

Brilliance
Research of Artificial Intelligence

E-ISSN : 2807-9035
Volume 6, **Number** 4, November 2026
https://doi.org/10.47709/brilliance.v6i4.9749

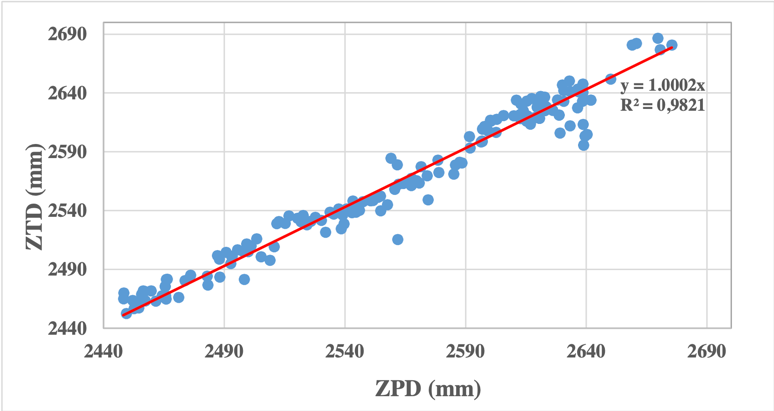


Figure 6. ZPD-ZTD scatter plot at several stations.

To visualize the similarity, a scatter plot (Figure. 6) was generated to determine the magnitude of the correlation between these two variables. Calculations using linear regression yielded a correlation of 98.21% with an RMS error of 1.79 mm.

Table 4. ZTD and ZPD Validation Results Data

Stations											
CBAL 050		**CBAL 051**		**CBAL 052**		**CSLU 050**		**CSLU 051**		**CSLU 052**	
ZTD	**ZPD**	**ZTD**	**ZPD**	**ZTD**	**ZPD**	**ZTD**	**ZPD**	**ZTD**	**ZPD**	**ZTD**	**ZPD**
2557,5	2545,0	2533,4	2448,7	2557,5	2538,7	2602,0	2557,5	2448,7	2557,5	2557,5	2448,7
2547,5	2544,3	2533,7	2558,7	2547,5	2538,7	2669,1	2547,5	2558,7	2547,5	2547,5	2558,7
2534,5	2545,0	2593,1	2668,7	2534,5	2448,7	2560,0	2534,5	2668,7	2534,5	2534,5	2668,7
2556,7	2785,9	2533,7	2558,0	2556,7	2558,7	2656,0	2556,7	2558,0	2556,7	2556,7	2558,0
2547,8	2545,0	2533,3	2552,9	2547,8	2668,7	2544,0	2547,8	2552,9	2547,8	2547,8	2552,9
2544,0	2578,4	2533,7	2098,7	2544,0	2558,0	2557,5	2544,0	2098,7	2544,0	2544,0	2098,7
2557,5	2557,5	2993,8	2390,7	2557,5	2552,9	2768,5	2557,5	2390,7	2557,5	2557,5	2390,7
2768,5	2547,5	2533,7	2239,0	2768,5	2098,7	2656,6	2768,5	2239,0	2768,5	2768,5	2448,7
2656,6	2534,5	2897,9	2558,5	2656,6	2390,7	2357,5	2656,6	2558,5	2656,6	2656,6	2558,7
2357,5	2556,7	2657,0	2558,2	2357,5	2239,0	2457,5	2357,5	2558,2	2357,5	2357,5	2668,7
2457,5	2547,8	2533,7	2558,7	2457,5	2538,7	2557,5	2457,5	2558,7	2457,5	2457,5	2558,0
2557,5	2544,0	2533,7	2558,4	2557,5	2538,7	2544,0	2557,5	2558,4	2557,5	2557,5	2552,9

Source: Results of ZTD and ZPD processing from CBAL and CSLU stations, 2025.

The scatter plot (Figure 6), Overall, the scatter plot and station-based validation tables provide complementary evidence for evaluating the performance of the linear regression approach. The scatter plot offers a visual representation of the agreement between estimated and reference values, whereas the tabulated results provide quantitative information for comparing the retrieval performance at CBAL and CSLU. Nevertheless, the reported correlation and RMS error should be interpreted together with the individual station results, the number of validation samples, and the characteristics of the reference measurements to ensure a comprehensive assessment of the method's accuracy and applicability. Representing calculations based on linear regression, shows a correlation of 98.21% with an RMS error of 1.79 mm. The validation results for both stations (CBAL and CSLU) are presented in the table above, accompanied by a more detailed explanation. These validation results can also be viewed in the table below.

Table 5. Average Validation Results at Stations CBAL and CSLU

Stations	Difference	Regresi	
	Std (Mm)	Rmse (Mm)	Kolerasi
CBAL	20,986	1,79	0,982
CSLU	19,678	4,23	0,975
Average	20,220	3.01	0,946

From Table 5. above, it can be seen that the standard deviation (std) value is 20.220 mm and the correlation is 0.946. Based on these values, it can be concluded that the ZTD derived in this study shows a high level of agreement with the IGS ZPD values. The discrepancy between the ZTD obtained from GPS data processing and the IGS ZPD values may stem from differences in GPS data processing methods (Karabatic, 2011; Susilo, 2012). These methodological differences include: temporal differences in ZTD estimation (ZTD in this study was estimated every 2 hours and 30 minutes, whereas ZPD is estimated every 2 hours); differences in GPS data processing software

This is an Creative Commons License This work is licensed under a Creative Commons Attribution-NonCommercial 4.0 International License.

Brilliance
Research of Artificial Intelligence

E-ISSN : 2807-9035
Volume 6, **Number** 4, November 2026
https://doi.org/10.47709/brilliance.v6i4.9749

parameters (GAMIT software was used for ZTD estimation in this study, while Bernese software is used for ZPD estimation); and differences in orbit parameters (orbit parameters were fixed in this study, whereas IGS includes them in the estimation). Based on these results, it is concluded that the ZTD determination technique/method employed in this study is optimal.

Precipitable Water Vapor (PWV) Results from TERRA MODIS Satellite Imagery

In general, PWV values estimated from Terra MODIS data using absorption channels (17, 18, and 19) and non-absorption channels (2 and 5) can be used to monitor weather conditions across various regions of Sumatra. The PWV distribution patterns for the study locations are presented in the following table:

Table 6. PWV results from TERRA MODIS satellite data

Doy	Min	Max	Std	The Mean Value Of Pwv (cm)	Date	Information
151	1,667	4,876	0,987	3,456	31 May 2025	Before
157	0,786	4,009	2,678	2,345	6 Juni 2025	
158	0,990	4,986	1,456	3,223	7Juni 2025	
159	0,765	6,657	0,234	3,445	8 Juni 2025	
167	0,453	6,678	0,098	3,234	16 Juni 2025	
042	1,768	5,098	1,987	2,445	11 Maret 2026	After
050	2,098	5,554	1,567	4,112	20 Maret 2026	Fire
051	0.887	5,345	2,876	4,334	21 Maret 2026	
052	0,546	7,657	1,223	3,221	22 Maret 2026	
058	0.678	7,567	2,234	2,456	27 Maret 2026	Before
214	1,099	6,546	0,123	1,345	1 September 2026	Fire
222	1,989	5,456	0,344	0,987	9 September 2026	
224	0,980	4,234	2,234	0,998	10 September 2026	
230	2,001	4,123	1,654	1,098	17 September 2026	

Source: TERRA MODIS satellite image processing data

Form Tabel 6. Analysis of PWV distribution derived from TERRA MODIS satellite imagery covering the period from June 2025 to September 2026 (encompassing pre-fire, post-fire, and active fire conditions) reveals significant variations in PWV values (see Table 6.). On September 2026, coinciding with an intensification of forest fire activity, the average PWV level rose to 7.000 cm, a value notably higher than the daily average recorded on other dates. This phenomenon may be attributed to the forest fires spreading into the atmosphere and influencing the solar radiation reaching the Earth's surface.

In addition to examining PWV values from individual stations, a composite graph of PWV values derived from TERRA MODIS satellite imagery was generated to determine the precise total PWV.

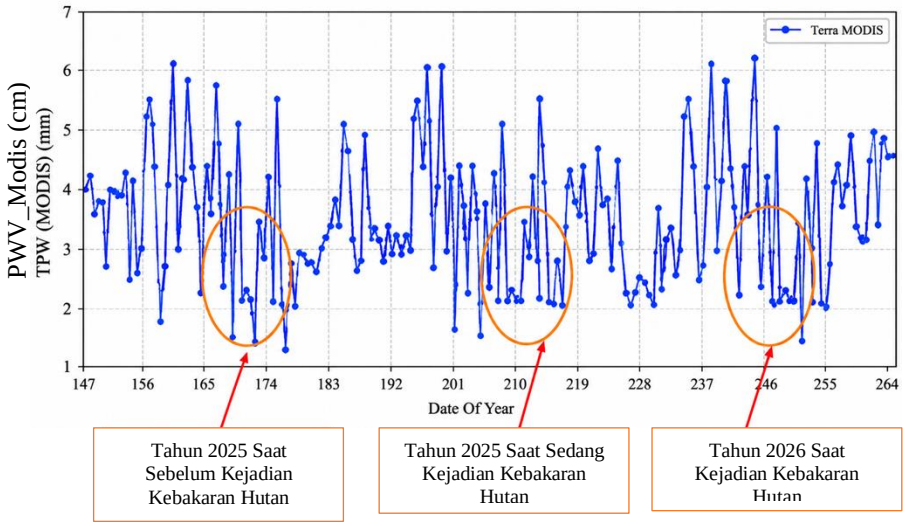


Figure 7. Graph of PWV values derived from TERRA MODIS satellite image data processing.

Figure 7. above illustrates the differences in PWV values derived from GPS data corrected using GAMIT software. Analysis of the GPS data indicates significant results, while data from TERRA MODIS satellite imagery using remote sensing techniques to measure PWV over Kalimantan during forest fires yielded a minimum value of 0.121 cm, a maximum value of 7.000 cm, a mean value of 2.308 cm, and a standard deviation of 1.325 cm.

This is an Creative Commons License This work is licensed under a Creative Commons Attribution-NonCommercial 4.0 International License.

Brilliance
Research of Artificial Intelligence

E-ISSN : 2807-9035
Volume 6, **Number** 4, November 2026
https://doi.org/10.47709/brilliance.v6i4.9749

Comparison of GPS PWV and MODIS PWV Data

To examine the strength of the relationship between PWV derived from GPS data processing and conventional PWV measurement techniques, this study employs two approaches: GPS technology applications and remote sensing techniques. The study analyzes the relationship between the two datasets specifically, TERRA MODIS imagery and GPS-derived PWV.

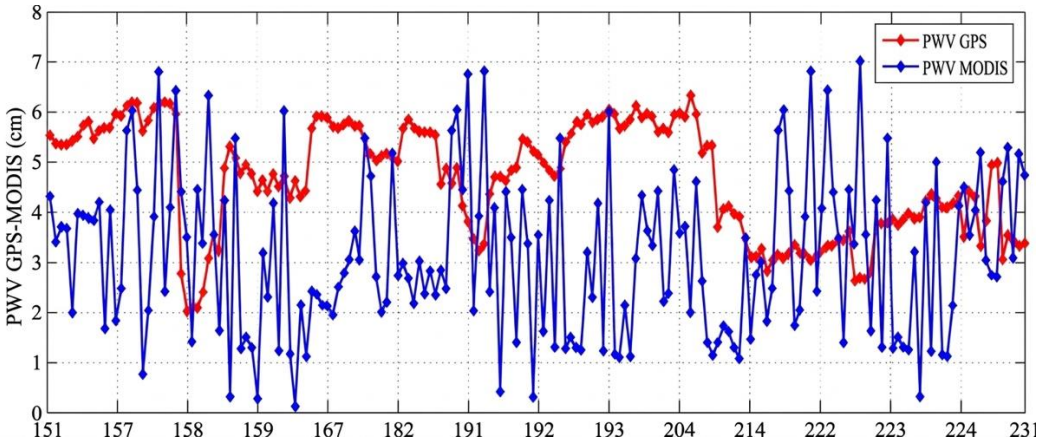


Figure 8. Comparison of GPS PWV and TERRA MODIS satellite imagery.

Figure 8. presents the PWV verification results, comparing PWV values estimated from MODIS data with those derived from GPS data. The standard deviation (std) values were 1.911 cm for the TERRA MODIS satellite imagery and 1.091 cm for the GPS data. Based on these values, it can be concluded that the GPS-derived PWV values obtained in this study show a high degree of agreement with the PWV values from TERRA MODIS satellite imagery.

DISCUSSION

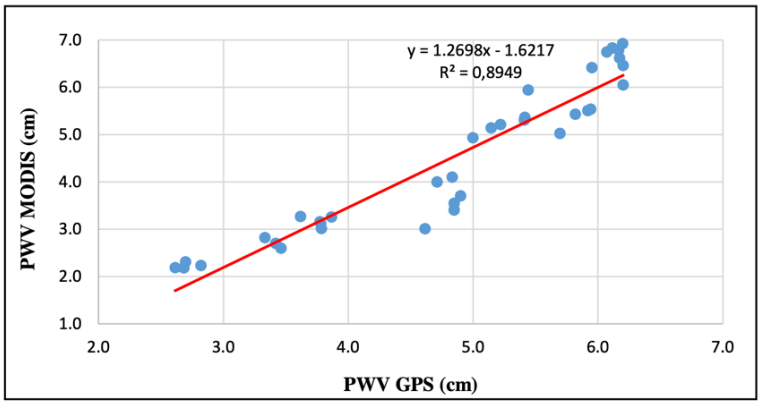


Figure 9. Scatter plot of PWV values (cm) from MODIS and GPS data Years 2025 and 2026.

Verification results for Precipitable Water Vapor (PWV) on Sumatra Island during the 2025 and 2026 periods indicate that PWV values estimated from MODIS data exhibit an average standard deviation of ±1.6 cm relative to GPS-derived PWV. Figure 4.28 illustrates the linear relationship between MODIS-derived PWV (x) and GPS-derived PWV (y), with a correction factor of 0.8949. Although the correlation (r) between MODIS-derived PWV and GPS-derived PWV is quite high at 89% MODIS estimates humidity levels in the range of approximately 54-77%, noting that PWV tends to decrease as terrain elevation increases. Consequently, as surface temperatures rise during forest fires, the surface temperature level shifts in a way that approaches the actual PWV value. Generally, humidity levels between 30% and 54% are considered acceptable and comfortable for humans; therefore, the forest fires affecting Sumatra Island significantly disrupt human activities. Regarding health impacts, forest fires cause air pollution including dust and gases such as SO2, NO2, and CO2 which can lead to adverse health effects such as respiratory tract infections, shortness of breath, skin irritation, and eye irritation.

This is an Creative Commons License This work is licensed under a Creative Commons Attribution-NonCommercial 4.0 International License.

Brilliance
Research of Artificial Intelligence

E-ISSN : 2807-9035
Volume 6, **Number** 4, November 2026
https://doi.org/10.47709/brilliance.v6i4.9749

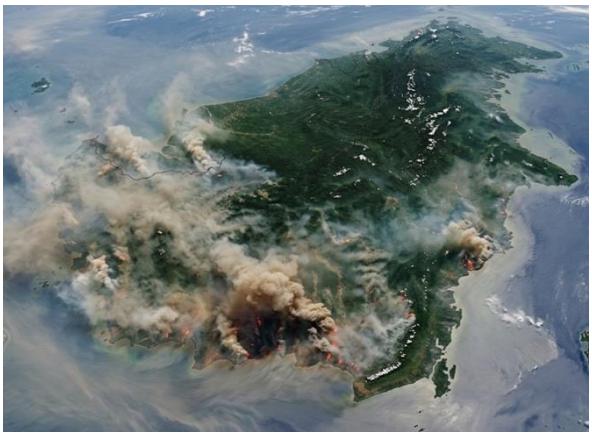


Figure 10. Terra MODIS Satellite Imagery During Forest Fires

CONCLUSION

Temporal variations in water vapor content at the study sites CBAL-CSLU ranged from approximately 3-8 cm/day (or around 89%).

Generally, across 2025 and 2026, the wettest month at the study locations was February, while the driest month was August. Precipitable Water Vapor (PWV) estimated from MODIS data shows a very high correlation ($r^2 = 0.8949$); PWV tends to decrease as regional topography rises and surface temperature increases. Generally, conditions acceptable to humans fall within the 30–54% range; however, when forest fires struck Sumatra, the recorded PWV value was 89%. MODIS estimated humidity at approximately 54-77%. Consequently, the forest fires affecting Sumatra significantly disrupted human activities.

Recommendations Based on the process and results of this study, the following recommendations are offered for future research to further develop this method for monitoring water vapor content: Further study is needed regarding real-time satellite orbits derived from GPS data. This would enable the water vapor monitoring system using this method to operate in real time. Further research on vertical distribution using the GPS Radio Occultation method is required. Additionally, further meteorological analysis based on the results of this study is needed.

ACKNOWLEDGMENT

The authors wish to thank the editorial team of Brilliance Journal (Sinta 3) for their support in publishing this research. Sincere appreciation is also extended to colleagues for their valuable assistance and technical writing support in completing this project.

REFERENCES

Anderson, H. (2022, September 20). Global Positioning System status and modernization [Conference presentation]. Civil GPS Service Interface Committee. https://www.GPS.gov/cgsic/meetings/2022/anderson.pdf

Baker, B. (2022, November 16). Military communications & positioning, navigation, and timing overview & GPS enterprise update [Conference presentation]. PNT Advisory Board. https://www.GPS.gov/governance/advisory/meetings/2022-11/baker.pdf

Feng, L., Zhang, T., Koh, T. Y., & Hill, E. M. (2021). Selected years of monsoon variations and extratropical dry-air intrusions compared with the Sumatran GPS Array observations in Indonesia. Journal of the Meteorological Society of Japan, 99(2), 505–536. https://www.jstage.jst.go.jp/article/jmsj/99/2/99_2021-026/_article

GPS.gov. (n.d.-a). What is GPS? https://gps.gov/systems/gps

Hsu, J., Chen, C.-A., Lan, C.-W., Chiang, C.-L., Li, C.-H., & Lo, M.-H. (2025). Impact of land use changes and global warming on extreme precipitation patterns in the Maritime Continent. npj Climate and Atmospheric Science. https://doi.org/10.1038/s41612-024-00883-z

Intergovernmental Panel on Climate Change. (2023). Climate Change 2023: Synthesis Report. Contribution of Working Groups I, II and III to the Sixth Assessment Report of the Intergovernmental Panel on Climate Change. IPCC. https://doi.org/10.59327/IPCC/AR6-9789291691647

Li, Y. (2021). Analysis of GAMIT/GLOBK in high-precision GNSS data processing for crustal deformation. Earthquake Research Advances, 1(3), 100028. https://doi.org/10.1016/j.eqrea.2021.100028

Lovita, O. (2017). Analisa Perubahan Cuaca Di Pulau Sumatera Akibat Kebakaran Hutan Dengan Data Water Vapor Dari Citra Satelit Terra Modis. Jurnal Inotera. https://inotera.poltas.ac.id/

This is an Creative Commons License This work is licensed under a Creative Commons Attribution-NonCommercial 4.0 International License.

E-ISSN : 2807-9035
Volume 6, **Number** 4, November 2026
https://doi.org/10.47709/brilliance.v6i4.9749

Ma, X., Yao, Y., Zhang, B., Qin, Y., Zhang, Q., & Zhu, H. (2022). An improved MODIS NIR PWV retrieval algorithm based on an artificial neural network considering the land-cover types. IEEE Transactions on Geoscience and Remote Sensing, 60, 1–12. https://doi.org/10.1109/TGRS.2022.3170078

Mustafovski, R., & Petrovski, A. (2025). State of the art on global navigation satellite systems: A comparative study of GPS, GLONASS, and Galileo. Contemporary Macedonian Defence, 25(49), 119–132. https://eprints.ugd.edu.mk/37256/

NASA. (n.d.). Terra & Aqua Moderate Resolution Imaging Spectroradiometer (MODIS). LAADS DAAC. https://ladsweb.modaps.eosdis.nasa.gov/missions-and-measurements/modis/

Su, H., Yang, T., Wang, K., Sun, B., & Yang, X. (2021). Evaluation of precipitable water vapor retrieval from homogeneously reprocessed long-term GNSS tropospheric zenith wet delay, and multi-technique comparison. *Remote Sensing*, *13*(21), 4490. https://doi.org/10.3390/rs13214490

Trakolkul, C., Charoenphon, C., & Satirapod, C. (2024). Investigating the relationship between precipitable water vapor and rainfall data during flood events: A GNSS-based study in Thailand. International Journal of Geoinformatics. https://ijg.journals.publicknowledgeproject.org/index.php/journal/article/view/3677

Vaquero-Martínez, J., & Antón, M. (2021). Review on the role of GNSS meteorology in monitoring water vapor for atmospheric physics. Remote Sensing, 13(12), 2287. https://doi.org/10.3390/rs13122287

Wang, Y., Yang, F., Li, P., Gong, X., Liu, M., Xu, T., Lin, X., & Wang, Y. (2024). An optimal calibration method for MODIS precipitable water vapor using GNSS observations. Atmospheric Research, 309, 107591. https://doi.org/10.1016/j.atmosres.2024.107591

World Meteorological Organization. (2025). WMO Greenhouse Gas Bulletin, No. 21. https://wmo.int/media/41825

Zhai, W., Zhu, J., Lin, M., Ma, C., Chen, C., Huang, X., Zhang, Y., Zhou, W., Wang, H., & Yan, L. (2022). GNSS data processing and validation of the altimeter zenith wet delay around the Wanshan calibration site. Remote Sensing, 14(24), 6235. https://doi.org/10.3390/rs14246235

Zhao, Y., Zhao, H., Li, J., & Xiao, G. (2022). Comprehensive validation and calibration of MODIS PWV over mainland China. Atmosphere, 13(11), 1763. https://doi.org/10.3390/atmos13111763

Zhu, D., Zhang, K., Yang, L., Wu, S., & Li, L. (2021). Evaluation and calibration of MODIS near-infrared precipitable water vapor over China using GNSS observations and ERA-5 reanalysis dataset. Remote Sensing, 13(14), 2761. https://doi.org/10.3390/rs13142761

This is an Creative Commons License This work is licensed under a Creative Commons Attribution-NonCommercial 4.0 International License.